minerals

MDPI

Article

Mechanism Study and Tendency Judgement of Rockburst in Deep-Buried Underground Engineering

Jiazhu Liu [1], Yongtao Gao [1,*], Fan Chen [2] and Zhensheng Cao [2]

[1] Key Laboratory of Ministry of Education for Efficient Mining and Safety of Metal Mines, University of Science and Technology Beijing, Beijing 100083, China
[2] Power China Road Bridge Group Co., Ltd., Beijing 100048, China
* Correspondence: gyt1962@163.com

Abstract: Rockburst is a type of dynamic instability failure phenomenon and frequently brings huge losses to underground engineering projects such as mines and tunnels. In order to explore rockburst mechanisms and predict rockbursts better, relying on the background of Wulaofeng deep-buried highway tunnel, in situ stress measurement was performed using new wireless devices, and mechanics tests of surrounding rock samples taken from different burial depths were carried out. The rockburst mechanism was explored from the microscopic perspective based on the analysis of scanning electron microscopy (SEM). Rockburst tendency was judged comprehensively by a tendency analysis, grade prediction and numerical simulation. The result showed that the mechanical parameters of granite rocks in the deep-buried section were larger than those in the entrance section, and the fractured morphology mainly comprised sheet and monolithic block, corresponding to transgranular fracture and intergranular fracture. Rocks with few types of mineral cementation, good crystallization and small particle size differences had better energy storage and release characteristics. There was little difference in the rockburst tendency of rocks with different buried depths, but there were obvious differences in the rockburst grade. In the deep-buried section of the tunnel, the rockburst grade was of a moderate–heavy level and the rockburst risk at the vault and right spandrel of the cross section was more severe, which was basically consistent with the situation at the tunnel site. This study can provide a theoretical basis for the prevention and control of rockbursts in Wulaofeng tunnel and other similar engineering projects.

Keywords: rockburst; underground engineering; numerical simulation; microcosmic mechanism; tendency judgement

Citation: Liu, J.; Gao, Y.; Chen, F.; Cao, Z. Mechanism Study and Tendency Judgement of Rockburst in Deep-Buried Underground Engineering. *Minerals* **2022**, *12*, 1241. https://doi.org/10.3390/min12101241

Academic Editor: Mamadou Fall

Received: 26 August 2022
Accepted: 20 September 2022
Published: 29 September 2022

1. Introduction

With the increase in mining depth and infrastructure projects, the construction environment has become more and more complex, and the disaster problems such as rockburst, coal-gas outburst and landslides have become more and more prominent [1–4]. Rockburst is a dynamic instability failure phenomenon, which is usually caused by the sudden release of the accumulated elastic energy of deep rock mass in high stress environment [5–7]. The surrounding rock mass is catapulted, thrown or even ejected into the excavated space suddenly and violently, which can result in great casualties and property losses. For example, extremely intense rockburst events occurred in Jinping Hydropower Station [8] and in Hanjiang-Weihe River Diversion Project [9], which destroyed the construction tunnels and took heavy tolls. Rockburst disasters tend to increase in tunnels that are growing in scale and depth [10,11]. Thus, the studies on the mechanism and prediction of rockburst have became research hotspots, which is very urgent and meaningful to improve construction safety [12].

It is generally recognized that internal and external conditions are both needed for a rockburst, that is, rock can accumulate enough energy, and construction disturbances

in high stress environments lead to a sudden release of energy. To prevent and control rockbursts effectively, considerable efforts have been made to explore their failure mechanism. Through the study and analogy of rock experiments, Gu et al. [13] divided the development process of rockburst into three stages: splitting into plates, cracking into blocks and rock mass ejection, and put forward the criterion for the occurrence of rockburst; Li et al. [14,15] regarded the development of rockburst as a process of energy accumulation and release, and divided it into three stages: energy accumulation, micro-rupture formation and expansion, and rupture surface penetration and burst ejection; Xu et al. [16,17] analyzed the characteristics of rock failure instability based on a triaxial unloading test, and explored the occurrence mechanism of rockburst. Ma et al. [18] attributed the root cause of rockburst to the non-uniformity and joints of the rock by microseismic detection and sonar localization, and analyzed the location of rockbursts. Wang et al. [19] analyzed the influence of structural surface factors on rockbursts based on UDEC software and microseismic monitoring. Luo et al. [20–22] conducted studies on the influence of temperature on rockbursts to investigate the stress involution and rockburst mechanisms in geothermally rich areas. He et al. [23] thought that rockburst was the phenomenon of dynamic instability, and conducted dynamic loading tests to study rockburst occurrence mechanisms under different circumstances. In summary, great progress has been made in the study of rockburst mechanisms. However, due to the complexity and uncertainty of the rockburst problem, the rockburst mechanism is still not clear, and it is mostly studied from a macroscopic perspective. In addition, it is difficult to obtain rocks at the site of rockburst disasters, so it is more meaningful to study them.

Based on the study of rockburst mechanisms, numerous scholars think that rockburst is predictable and have conducted much specific research on rockburst tendency [24–26]. In general, the evaluation methods of rockburst tendency can be divided into three categories: empirical analysis, theoretical analysis and numerical simulation. The empirical analysis is mainly based on the empirical indicators of rockburst, including single indicators and multiple indicators [27]. Qu et al. [28] conducted a rockburst tendency analysis on the deep-buried tunnel based on lithological conditions; Wu et al. [29] studied the rockburst tendency of various rocks with four indicators comprehensively: rock mass brittleness index, elastic deformation energy index, impact energy index and residual energy index. In recent years, Zhang et al. [30,31] put forward some new indexes or modified traditional rockburst criteria to make the index further enriched. Theoretical analysis mainly refers to propensity analysis through mathematical theory and machine learning, including fuzzy mathematics, rough set, unsupervised learning, linear classification models, decision trees, neural network and so on [32–37]. Besides, as a convenient and high-efficiency tool, numerical simulations have been widely used in the problem analysis of rockburst tendency. There are three main numerical methods: continuum method, discontinuum method, and hybrid method [38]. For instance, Hatzor et al. [39,40] used discontinuous deformation analysis (DDA) method and combined with methods such as GSI to assess rockburst tendency. Nowadays, the hybrid method is used more in related analyses. Overall, many studies about tendency analysis have been done, but they are mostly vague evaluations of large areas that are not very targeted, and the results of indoor analysis and on-site analysis are used confusingly without a clear distinction. Moreover, the tendency analysis is not systematic and does not provide a strong guidance to the site.

In this study, based on the Wulaofeng deep-buried highway tunnel, the occurrence mechanism of rockbursts was analyzed from a microscopic point of view, and rockburst tendency was judged comprehensively by three stages. Firstly, the characteristics of in-situ rockbursts were analyzed, geo-stress measurements were carried out with new wireless measuring device, and rock mechanics tests, in which rock samples were obtained from different burial depths of the site, was conducted. Rockburst mechanisms wes then explored in terms of fracture topography and composition from a microscopic perspective using SEM. Subsequently, rockburst tendency was judged by theoretical analysis which is divided into tendency analysis and grade predition. Finally, relying on numerical simulation and limit

energy criterion, the rockburst tendency of different positions of the tunnel was analyzed from the perspective of energy accumulation, making the analytical results more targeted.

2. Project Overview

2.1. Engineering Background

Wulaofeng Highway Tunnel is a typical deep-buried long mountain tunnel, which is located in Yunnan Province, China, with a maximum burial depth of 929 m and nearly 60% of which is more than 400 m buried. The tunnel section is a straight-wall–top-arch type with size of 12.0 × 8.5 m^2. The lithology of the tunnel is dominated by hard granite, and as the construction progresses, some rockbursts have appeared. Judging from the in-site investigation, the rockbursts mainly occurred in the tunnel heading face, vault and spandrel, which were initially judged to be weak- and moderate-intensity rockbursts. The geographical location of Wulaofeng Project is shown in Figure 1.

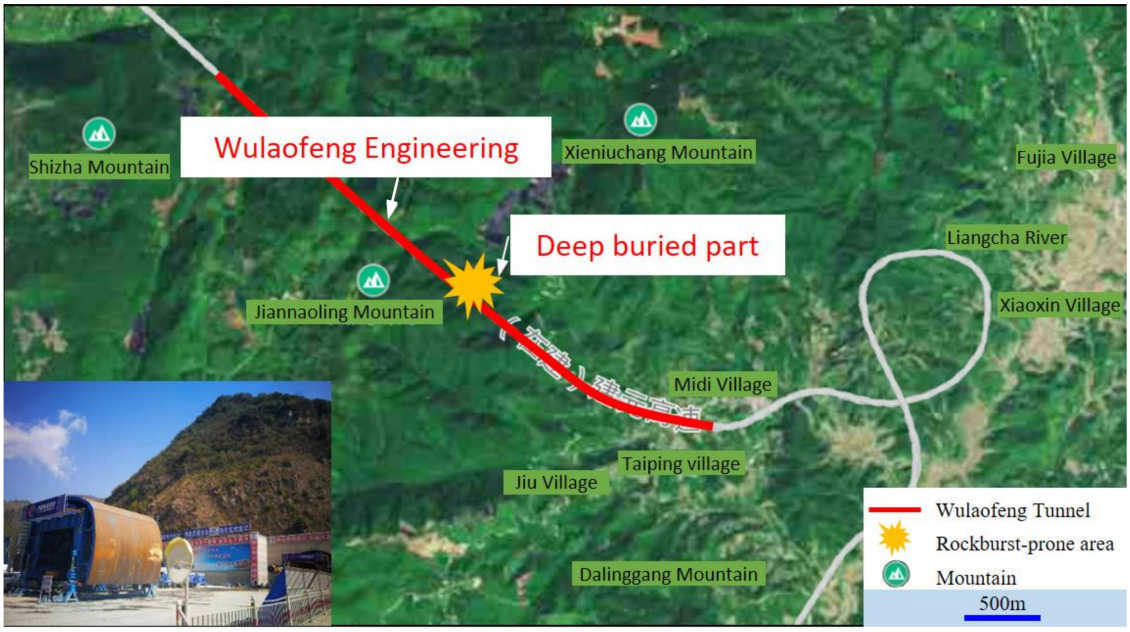

Figure 1. The geographical location of Wulaofeng Engineering.

2.2. Rockburst Characteristics

As tunnel construction progressed, the phenomena of high geostress began to appear. For example, drilling pipesticking happens frequently when drilling. Correspondingly, rockbursts occur in the tunnel, which seriously interferes with normal construction operations.

The locations of rockbursts are mainly in the palm surface, vault and right spandrel, where the falling rocks show different forms such as flakes, plates, small blocks, and large blocks, mainly flakes and plates. According to the research conclusion of Feng et al. [7], the depth of the blasting pit, the length along the axis of tunnel, the characteristics of the blasting block and other aspects of rockbursts were observed on the site, and the rockburst intensity was divided. The largest rockburst pit reaches a depth of 2 m, and the intensity of the rockbursts varies from slight to strong. Rockbursts occur mainly in granite and a small part in limestone.The integrity of the surrounding rock is Grade III or IV, and the construction method used is the full-section method or the step method.

Figure 2 shows photos of some rockburst damage. Figure 2a shows a weak rockburst that catapulted or flaked in the form of flakes, accompanied by a crisp tearing sound; Figure 2b,c is moderate rockbursts, showing plate-like or block-like destruction, of which the rockburst in Figure 2b was plate-like catapults, with a plate thickness of about 10 cm, accompanied by a bursting sound; Figure 2d shows the heavy rockburst that appeared, throwing a large amount of plate-like and blocky surrounding rock, and the pit reached a depth of 1.5 m.

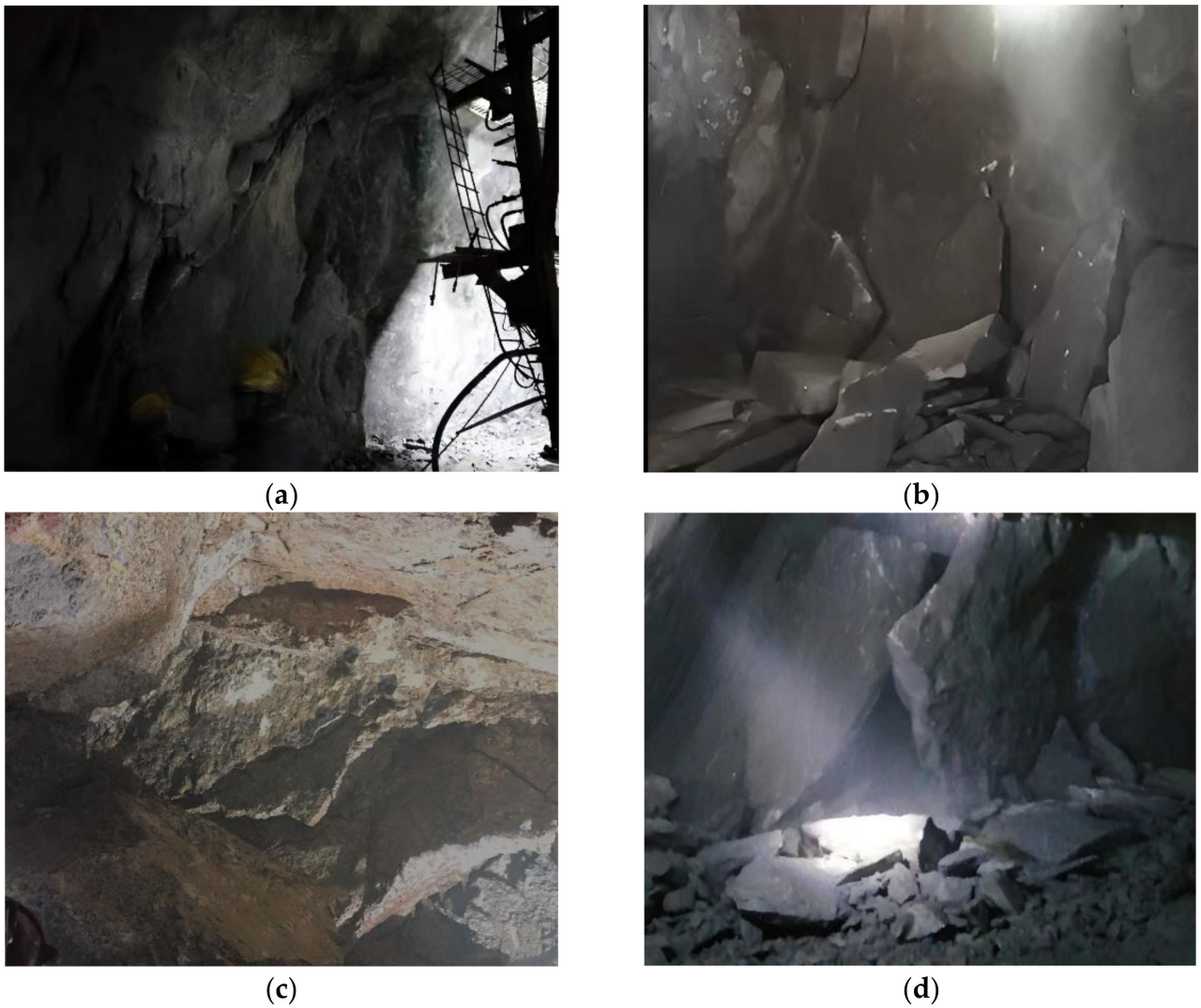

Figure 2. Rockburst phenomena on the site: (**a**) Weak rockburst; (**b**) moderate rockburst; (**c**) moderate rockburst; (**d**) heavy rockburst.

2.3. In Situ Stress Measurement

On the site, an in situ stress measurement was carried out using the new wireless instantaneous continuous acquisition hollow envelope strain gage of the academician Cai Meifeng's team, and the core of the hollow envelope is shown in Figure 3. When compared with the traditional hollow envelope strain gage, the new equipment overcomes the problems of signal attenuation caused by long wires in the measurement process and twisting of the wire by the drill pipe. In addition, the power-off continuous mining technology used has many advantages. It not only eliminates the problem that the acquisition system will heat up and affect the measurement accuracy during the long-term measurement process of the traditional probe, but also ensures that the test and monitoring process can be continuously and effectively collected, which can make the geo-stress measurements more accurate and convenient. Figure 4 shows the drilling operation in the field by a geological rig in April 2020. The measurement point was set up at the widened section with a depth about 900 m (chainage k27 + 960).

The measurement process is divided into five steps: (a) drilling large holes, grinding the bottom of the holes; (b) drilling concentric holes and cleaning up the chips; (c) installation of a measuring probe in the center of the small hole; (d) relieving the stress of the nested core; (e) calculating the original rock stresses.

Figure 3. A core that envelops a hollow inclusion.

Figure 4. Drilling operation in the field.

Each measuring point has 12 strain gauges, which can collect strains in 12 directions, and perform double temperature compensation for strain rates of each gauge. The ground stress component is then obtained based on the least squares fitting method. After ground stress measurement and inversion, the ground stress field of the measured lot is obtained, of which the deep-buried lot is dominated by horizontal ground stress. The principal stress values of the above measured point is shown in Table 1. The maximum stress value reaches 37–40 MPa, which belongs to the high-stress level.

Table 1. Meaurement results of principal stresses.

Stress Factors	The Maximal Principal Stress	The Intermediate Principal Stress	The Minimum Principal Stress
Value/MPa	38.27	24.94	23.11
Direction	−36.82	−19.34	54.94
Inclination/°	−18	71	−5

3. Rock Properties and Rockburst Mechanism

3.1. Experimental Study of In Situ Rocks

The rock samples were collected from Wulaofeng area at the depth of 110 m at the entrance and the depth of 850 m where the rockbursts happened. Standard cylindrical specimens with dimensions of 50 mm × 100 mm were prepared from the collected rock blocks. Specimen numbers are shown in Table 2. Regarding the serial number: WLF is an abbreviation of WLF. U, L, and B represent the test type (U—uniaxial compression,

L—loading and unloading, B—Brazilian). S and D represent depth of rock (S—shallow, D—deep). The total stress–strain curve of rock deformation failure was obtained by a uniaxial compression test, and the type and mechanical properties of rock failure were analyzed. The release energy and loss energy of rock were obtained by uniaxial loading and unloading test, and the elastic strain energy characteristics of rockbursts were analyzed. The tensile properties of rocks were studied through the Brazilian Split test.

Table 2. Number of rock mechanics test samples.

Type of Test	Specimen Source	Serial Numble	Specimen Source	Serial Numble
Compression test	Entrance section	WLFUS-01-1 WLF-US-01-2 WLF-US-01-3	Deep buried section	WLF-UD-02-1 WLF-UD-02-2 WLF-UD-02-3
Loading and unloading test	Entrance section	WLF-LS-03-1 WLF-LS-03-2	Deep buried section	WLF-LD-04-1 WLF-LD-04-2
Brazilian test	Entrance section	WLF-BS-05-1 WLF-BS-05-2 WLF-BS-05-3	Deep buried section	WLF-BD-06-1 WLF-BD-06-2 WLF-BD-06-3

3.1.1. Whole Process Test of Rock Deformation and Failure

In this test, a total of 6 cylindrical specimens were selected, including 3 specimens from the entrance and 3 specimens from the deep burial section. Using the combined control mode of displacement and pressure, the test was first loaded in a pressure control mode of 500 N/s, and the loading was stopped when the sample began to yield. Then, the mode was transformed into displacement control, with a rate of 0.02 mm/min until the sample was destroyed. The stress–strain curves obtained by the test are partially shown in Figure 5, and the calculated physical and mechanical parameters are shown in Table 3, Where ε_F and ε_B represent the pre-peak strain and post-peak strain, and W_E and W_P represent accumulated energy and released energy. Besides, S and D represent the depth of rock (S—shallow, D—deep).

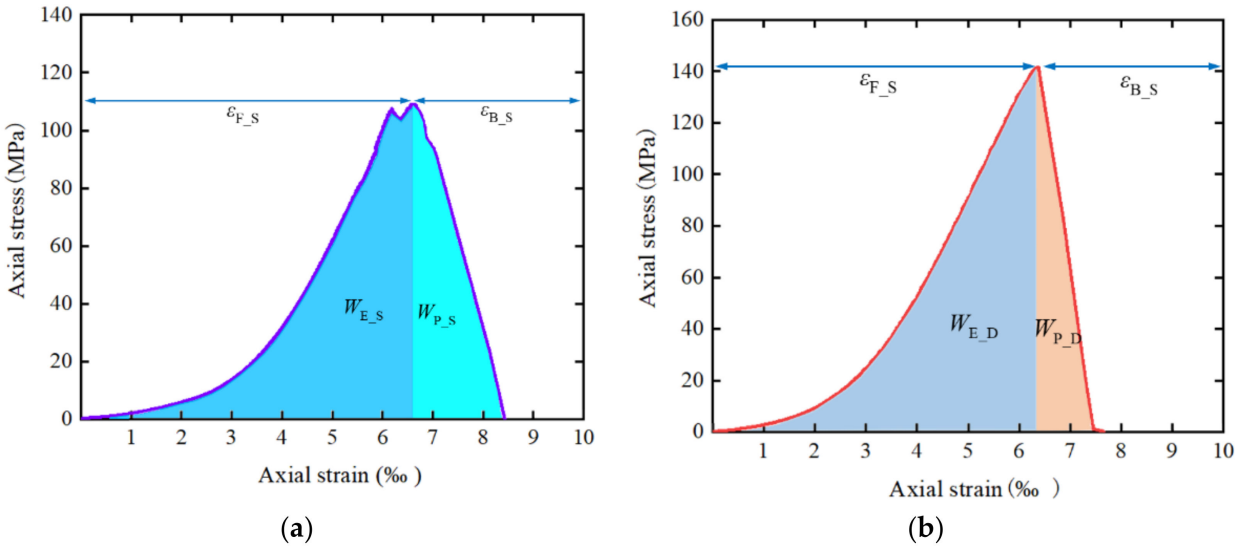

Figure 5. Stress–strain curves of granite specimen: (**a**) Entrance section; (**b**) Deep buried section.

From the test results, it can be seen that the granite of the Wulaofeng Tunnel shows obvious brittle failure characteristics. The average compressive strength of the deep-buried section is 134 MPa, which is greater than the strength at the entrance section that is 106 MPa. The elastic modulus of the deep-buried section is 35 GPa and the Poisson ratio is 0.22, which are also slightly larger than the entrance section. At the stage of crack closure and compaction, the stress–strain curve appears to be obviously concave, indicating there exist many original microcracks in the rock and the porosity is large. Moreover, obvious uneven

coarse particles can be seen in the specimen, which will also have a certain impact on the physical and mechanical properties of the granite.

Table 3. Results of uniaxial compression test.

Sample Source	Serial Number	Uniaxial Compression Strength (UCS)/MPa	Elasticity Modulus/GPa	Poisson's Ratio	Failure Mode
Entrance section	WLF-US-01-1	124.38	33.12	0.21	tensile
	WLF-US-01-2	92.23	26.67	0.17	tensile
	WLF-US-01-3	102.17	29.85	0.20	tensile/shear
	mean value	106.26	29.89	0.19	
Deep buried section	WLF-UD-02-1	131.74	32.55	0.21	tensile
	WLF-UD-02-2	144.62	35.36	0.23	tensile
	WLF-UD-02-3	126.42	37.42	0.23	tensile
	mean value	134.26	35.11	0.22	

The specimens after partial destruction are shown in Figure 6.

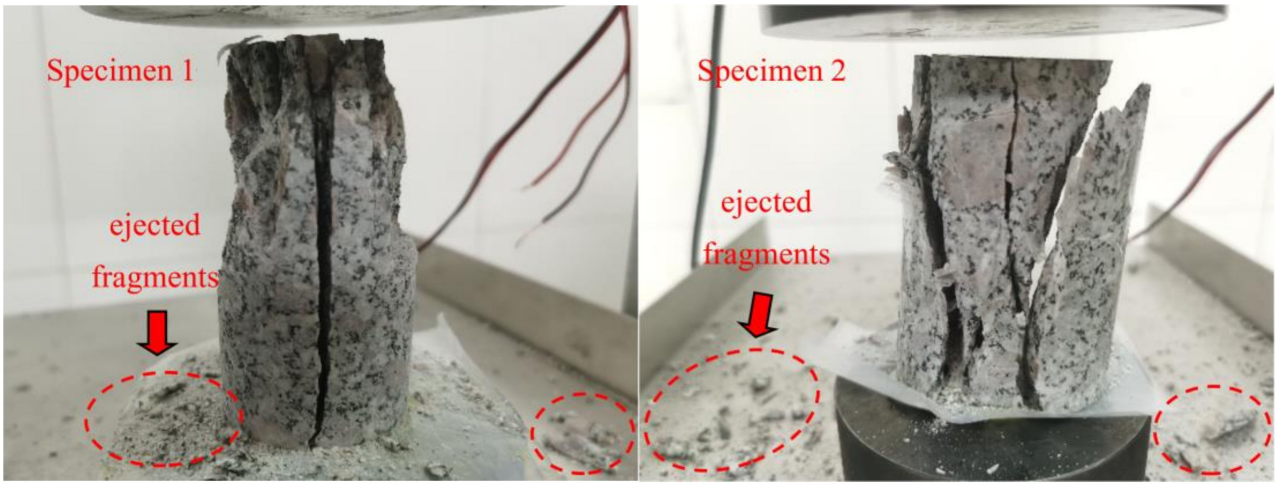

Figure 6. The specimens after tests.

The specimens from the deep-buried section all show significant tensile failure. For the specimens from the shallow-buried section, the first two show tensile failure and the third specimen shows a mixed failure of tensile and shear. It was also found that the tensile failure changed at the position where there are large blocks, i.e., an uneven block will affect the direction of crack expansion. When doing the test, there was an obvious phenomenon of fragment ejection, which was scattered on the test bench around the specimen, indicating that the falling fragments had a certain ejection kinetic energy. Meanwhile, the test was accompanied by different degrees of crackling sounds, which is equivalent to different degrees of rockburst destruction.

3.1.2. Uniaxial Loading and Unloading Test

The loading and unloading test was conducted so as to analyze the characteristics of energy storage and dissipation. Firstly, the rock sample was loaded axially at a rate of 500 N/s, and the compression was stopped when the load reached 70%–80% of the compressive strength, that is, about 90 MPa. Then, the pressure was unloaded, and the hysteresis loop was obtained. The stress–strain curves of the test are partially shown in Figure 7, where W_{st} and W_{sp} represent dissipated energy and released energy, respectively. It is seen that the inelastic deformation and the plastic hysteresis are both obvious; especially in the deep-buried granite it is more prominent. The dissipated energy in Figure 7a is larger than that in Figure 7b. But for every specimen, the energy difference between dissipation

and release is not obvious. All in all, the rock from the deep-buried section will release more energy than that from the entrance section.

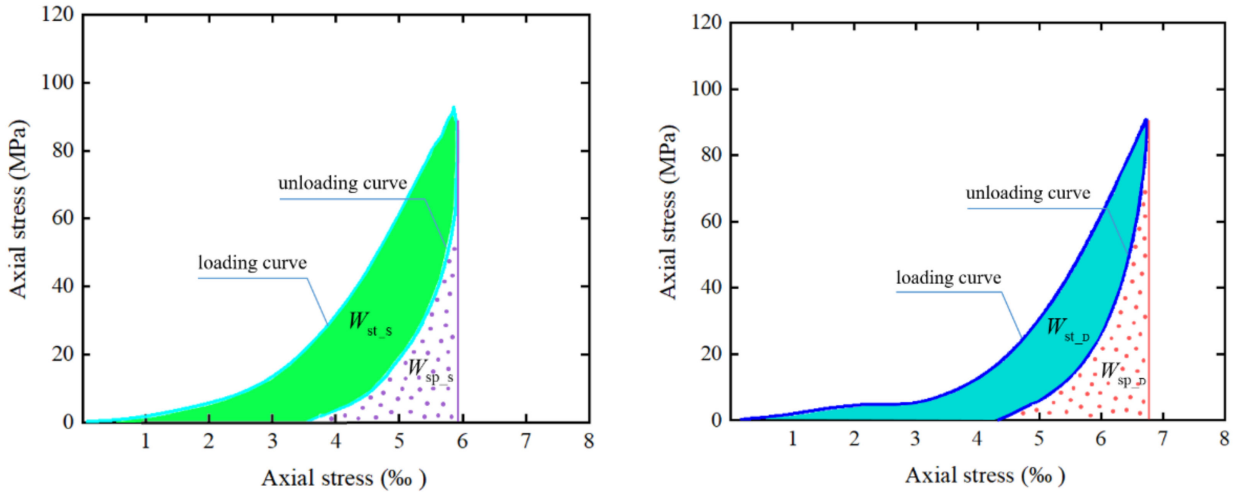

Figure 7. Test curves of uniaxial loading and unloading. (**a**) From entrance section. (**b**) From deep-buried section.

Then, the Brazilian Split test was carried out on the processed specimens. The average tensile strength of the deep-buried section was 9.5 MPa, while the entrance section was 6.7 MPa.

3.2. Microscopic Mechanism Analysis of Rockburst

In order to study the microscopic mechanism of rockbursts, SEM was used to scan the vertical fractures of rocks from the deep-buried section and the entrance section (numbered 2–3 and 1–3, respectively). Through the observation and analysis of the morphology of rock fractures, the characteristics and mechanisms of rock fractures were studied. By analyzing the composition of components, the rockburst mechanism was explored from the microscopic composition.

3.2.1. Analysis of Fracture Topography

Rock fracture morphology is divided into two types: tension fracture and shear fracture [41], corresponding to tensile failure and shear failure. Typical broken morphology mainly includes: river-like, complete block-shaped, step-shaped, honeycomb-shaped, fishbone-like, fog-like area-like and so on. Among them, from the perspective of fracture mechanism analysis, intergranular fracture (intact particle fracture) and transgranular fracture (cleavage fracture) are the main microscopic fracture modes of tensile failure, while slip fractures and microporous aggregation fractures are the main modes of shear failure [42].

Through SEM analysis, it can be seen that the main fracture morphology of the samples comprise flaky structures and block structures, as shown in Figure 8. Figure 8a is a layered structure consisting of flake minerals. Under the action of external loads, cracks occur easily between layers. Due to the presence of interlayer material and the non-uniformity of the mineral composition, the cracks change the direction of expansion. Eventually, tearing appears, forming a schematic fracture. During this process, a transgranular fracture occurs, which manifests as tension failure. Figure 8b shows a block structure with good integrity. Granite is composed of different mineral crystals, which are enriched by other cementitious substances. Due to differences in strength, cracks are easy to occur between the grains when the rock is subjected to the action of force. As the cracks continue to develop, eventually failure appears along the crystals. The composition of the complete block structure in Figure 8b is quartz, which has a high content in the rock and has a large impact on the

breaking of the rock. When the failure occurs at this place, it is mainly manifested as the fracture along the intact particles illustrated. The broken section is parallel to the direction of the principle stress, and the macroscopic manifestation is that of tensile failure.

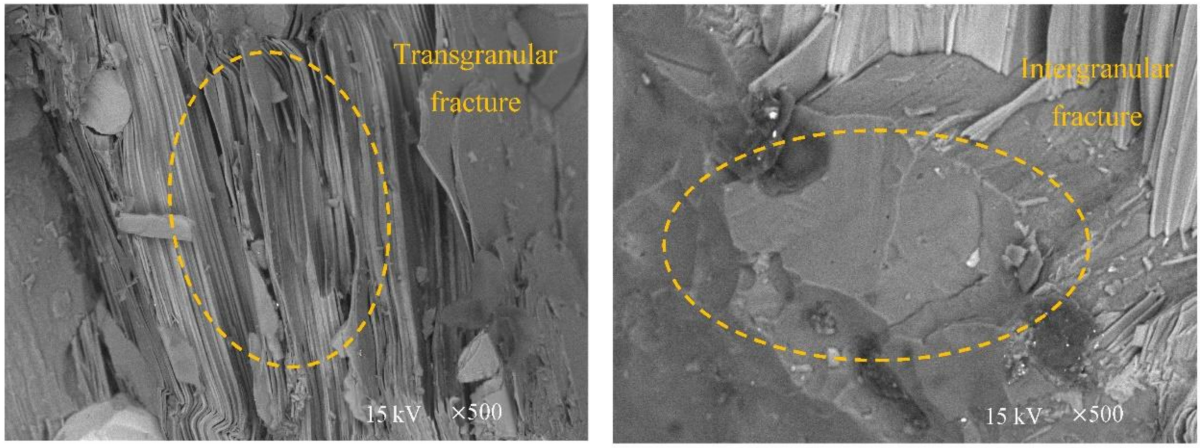

(**a**) (**b**)

Figure 8. Scanning morphology of the fracture. (**a**) Foliated structure; (**b**) Block structure.

3.2.2. Mechanism Study Based on Microscopic Components

In essence, the microscopic composition and structure of rock determine its macroscopic mechanical properties. Rock is a collection of minerals, and the physical and mechanical properties of rocks will be affected by different components, so that the properties such as rock brittleness, energy storage characteristic will be different. In order to study the correlation between microscopic composition of granite and rockbursts, the microscopic composition analysis of the two observation samples above was carried out. The EDS spectra are shown in Figure 9, and the sample compositions are shown in Tables 4 and 5.

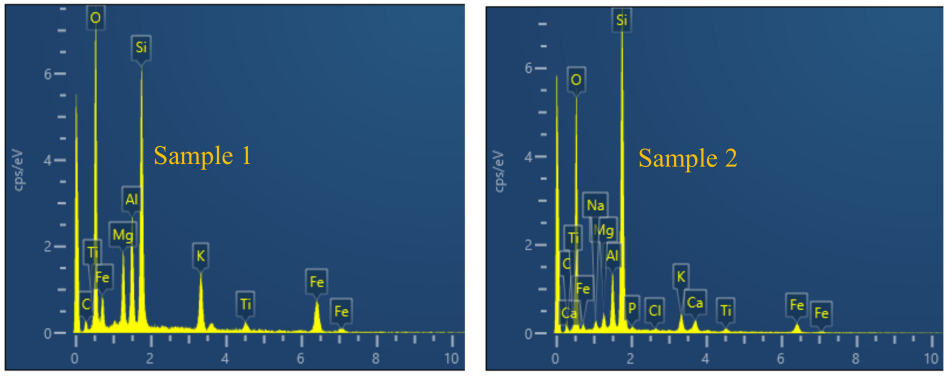

Figure 9. EDS spectrum.

Table 4. Composition of Sample 1.

Chemical Element	Percentage by Weight	Wt/% (Variance)	Atomic Percentage
Fe	12.29	0.42	4.57
O	55.99	0.55	72.73
Al	6.13	0.19	4.72
Si	14.42	0.27	10.67
K	5.28	0.17	2.80
Mg	4.61	0.18	3.94
Ti	1.30	0.15	0.56

Table 5. Composition of Sample 2.

Chemical Element	Percentage by Weight	Wt/% (Variance)	Atomic Percentage
Fe	4.74	0.21	1.67
O	60.67	0.34	74.70
Al	3.93	0.10	2.87
Si	23.47	0.23	16.46
Mg	1.20	0.07	0.97
K	2.18	0.08	1.10
Ca	1.62	0.08	0.80
Na	0.97	0.09	0.83
Ti	0.72	0.08	0.30
P	0.31	0.05	0.20
Cl	0.19	0.04	0.10

Combined with chart analysis, it can be seen that: (1) Sample 1 contains a total of seven elements (Fe, O, Al, Si, K, Mg, Ti), and Sample 2 contains a total of ten elements, with an addition of four elements, Ca, Na, P, and Cl. In contrast, Sample 1 has better particle size uniformity and a higher degree of crystallization. (2) From the perspective of mineral composition, the samples contain lots of quartz, and the presence of quartz will increase the brittleness and energy storage characteristics of the rock, making the sample rocks show high brittleness and energy storage characteristics. Mica, which has a low strength and is easy to stretch or tear off, has a significant impact on the initial breaking of rock. (3) In the case of small difference of main component, the cementation type, crystallization degree and particle size difference of minerals will have a major impact on the energy storage and release characteristics of the rock, and the grain structure of the minerals has an important influence or even a decisive effect on the strength in the brittle failure of rock.

4. Comprehensive Judgment of Rockburst Tendency

4.1. Analysis of Rockburst Tendency

Tendency analysis mainly refers to rockburst evaluation through rock indicators obtained from indoor rock mechanics tests. There are many evaluation indicators; the main ones commonly used are the elastic deformation energy index, energy storage and consumption coefficient, energy impact index, brittleness coefficient, etc. The following takes the brittleness coefficient as an example to analyze the rockburst tendency of rock.

The so-called brittleness coefficient criterion refers to the use of the ratio of rock compressive strength to tensile strength to evaluate the rockburst tendency, and its expression is:

$$B = \sigma_c / \sigma_t \tag{1}$$

where B is the brittleness coefficient. the criteria is:

$$\begin{cases} B > 40 \quad (\text{no rockburst}) \\ 26.7 < B < 40 \quad (\text{weak rockburst}) \\ 14.5 < B < 26.7 \quad (\text{moderate rockburst}) \\ B < 14.5 \quad (\text{heavy rockburst}) \end{cases} \tag{2}$$

For the deep-buried section, based on rock strength, the B values were calculated to be 13.9, 15.3 and 13.2, corresponding to the rockburst tendency of heavy, moderate and heavy, respectively; For the shallow-buried section, the calculated B values were 18.5, 13.7 and 15.2, corresponding to the rockburst tendency of moderate, heavy and moderate, respectively.

Similarly, the linear elastic energy value, elastic deformation energy index, and energy storage and consumption index [43–45] were used to analyze the rockburst tendency, and the statistical results are shown in Table 6.

Table 6. Results of the judging of rockburst tendency.

Sample Source	Serial Number	Analysis of Rockburst Tendency				Prediction of Rockburst Grade	
		Linear Elastic Energy	Energy Impact Index	Energy Storage and Consumption Index	Brittleness Coefficient	Russense Criterion	Barton Criterion
Entrance section	US-01-1	heavy	heavy	moderate	moderate	no	no
	US-01-2	moderate	heavy	moderate	heavy	no	no
	US-01-3	moderate	no	moderate	moderate	no	no
Deep buried section	UD-02-1	heavy	heavy	moderate	heavy	heavy	weak
	UD-02-2	heavy	heavy	moderate	moderate	heavy	weak
	UD-02-3	heavy	moderate	moderate	heavy	heavy	moderate

4.2. Prediction of Rockburst Grade

Although the rockburst tendency has been analyzed through indoor rock tests, rockbursts can only occur when the rocks are in the specific stress environment [46]. Therefore, the Russense criterion based on the strength stress ratio [47] was selected to predict the rockburst level of engineered rock mass.

The Russense criterion was used to analyze the intensity of rockbursts in accordance with the relationship between the maximum tangential stress around the cave and the rock point load strength. Later, for the convenience of calculation, the point load strength was changed to a uniaxial compressive strength, and the discriminant relationship is as follows:

$$\begin{cases} \sigma_\theta/\sigma_c < 0.20 \quad (\text{no rockburst}) \\ 0.20 \le \sigma_\theta/\sigma_c < 0.30 \ (\text{weak rock burst}) \\ 0.30 \le \sigma_\theta/\sigma_c < 0.55 \ (\text{moderate rockburst}) \\ \sigma_\theta/\sigma_c \ge 0.55 \quad (\text{heavy rockburst}) \end{cases} \tag{3}$$

Through measurement and inversion, the maximum principal stress at the sampling point of the deep-buried section is 34 MPa, perpendicular to the tunnel axis. Based on elastoplastic mechanical calculations, the maximum tangential stress at the point is σ_θ = 83 MPa. The uniaxial compressive strengths of the known specimens are 132 MPa, 147 MPa and 126 MPa, respectively, and the calculations σ_θ/σ_c are equal to 0.63, 0.58, and 0.64, respectively. According to Russense' judgment, the rockburst at this site is of a heavy grade. Due to the shallow depth of the tunnel at the entrance section, the geo-stress is small. According to this method, it is judged that no rockburst would occur.

Similarly, the Barton criterion [48] was used for grade prediction. The statistics of the comprehensive evaluation results of rockburst tendency are shown in Table 6.

From the analysis of Table 6, it is known that: (1) Overall, rocks from different burial depths both show a certain rockburst tendency from moderate to heavy. The tendency of the deep buried rock is slightly larger than that at the shallow section, but the difference between the two is not too large. (2) The rockburst grades are different at two places: there is no rockburst at the entrance section, while the rockburst grade at deep-buried section varies from weak to strong. (3) Through the in-site investigation, it is learned that moderate-intensity rockbursts occur near the sampling point of the deep burial section, which is almost consistent with the results of tendency judging. The rock mass was ejected in a flaky manner with a cracking sound, which has a certain impact on safe construction. There is no rockburst predicted at the entrance section, mainly because the tunnel at the entrance is shallow and there exists more joint fissures, which makes the rock mass relatively broken and does not reach a certain degree of stress concentration.

5. Simulation Analysis Based on Energy Accumulation Theory

5.1. Rockburst Criterion Based on Limit Energy

Rockburst is a dynamic instability process produced by the sudden release of accumulated energy in rock mass, which is essentially a destructive phenomenon driven by

energy. Assuming that in a closed system, the total input energy is U, according to the laws of thermodynamics, then:

$$U = U^{\mathrm{d}} + U^{\mathrm{e}} \tag{4}$$

where U^{d} represents the dissipative energy that is irreversible, and U^{e} represents the releasable elastic strain energy of the element. The energy in the principal stress space [49] can be expressed as:

$$\begin{array}{c} U = \int_0^{\varepsilon_1} \sigma_1 \mathrm{d}\varepsilon + \frac{1}{2}\sigma_2\varepsilon_2^{\mathrm{e}} + \frac{1}{2}\sigma_3\varepsilon_3^{\mathrm{e}} \\ U^{\mathrm{e}} = \frac{1}{2}\sigma_1\varepsilon_1^{\mathrm{e}} + \frac{1}{2}\sigma_2\varepsilon_2^{\mathrm{e}} + \frac{1}{2}\sigma_3\varepsilon_3^{\mathrm{e}} \end{array} \tag{5}$$

where: σ_1, σ_2, σ_3 are the three principal stresses, and $\varepsilon_1^{\mathrm{e}}$, $\varepsilon_2^{\mathrm{e}}$, $\varepsilon_3^{\mathrm{e}}$ are the elastic strain energy in the direction of the three principal stresses.

The energy value required for element failure is counted as U^0, and its value is affected by factors such as containment pressure, unloading rate, etc. [50]. When $U^{\mathrm{e}} < U^0$, the element is not destroyed. When $U^{\mathrm{e}} = U^0$, the element is in a critically broken state. When the $U^{\mathrm{e}} > U^0$, the element undergoes dynamic destruction, and the destructive kinetic energy is $\Delta U = U^{\mathrm{e}} - U^0$. Therefore, the failure criterion of the element can be summarized as:

$$U^{\mathrm{e}} > U^0 \tag{6}$$

The surrounding rock is in a multidirectional stress state of space. Due to the different stress states in different places, the energy storage limit of the element is also different. The excavation and unloading of underground engineering will change the force of the element, which will also change the limit value, so the energy storage limit of different elements is different and dynamic. The energy U in the current state of the element is compared with its energy storage limit U^0, and different numerical intervals are divided, so as to realize the judgment of the rockburst tendency:

$$U/U_0 = \begin{cases} 0.2\ (\text{a little rib spalling, I, weak rock burst}) \\ 0.4\ (\text{severe rib spalling, II, moderate rockburst}) \\ 0.5\ (\text{demand–type support, III, strong rockburst}) \\ \geq 0.7\ (\text{severe damage, IV, heavy rockburst}) \end{cases} \tag{7}$$

The indicator U/U_0 can more easily express the energy level of different positions in the tunnel construction process, reflecting the degree of energy accumulation, and can be used to evaluate the rockburst tendency with the help of numerical calculation. Regarding the energy storage limit of rock, U^0, some scholars have conducted relevant research [51]. In this paper, considering different triaxial test conditions, the ultimate energy values of granite in Wulaofeng tunnel were statistically calculated, as shown in Figure 10. Fitted to obtain a limit energy expression:

$$U_0 = -4.840 \times 10^{-6}\sigma_3^3 + 1.749 \times 10^{-5}\sigma_3^2 + 0.037\sigma^3 + 0.271 \tag{8}$$

Since U^{d} is the dissipated energy of the element and is the irreversible energy consumed by plastic deformation and damage, U^{e} is approximated as U.

5.2. Numerical Simulation Analysis

5.2.1. Modeling and Calculation

The software FLAC3D (Version 5.0, Itasca Consulting Group, Minneapolis, MN, USA) was used to analyze the energy accumulation condition during the construction of Wulaofeng Tunnel. The rockburst section was selected with a burial depth of 850 m. In order to eliminate the boundary effect, the distance from the tunnel to the boundary was taken as about five times the diameter of the hole, and a 3D model as shown in Figure 11 was established. The model dimensions are 130 m × 42 m × 110 m, with the Y direction being the tunnel excavation direction and the Z-direction level equivalent to −800 m~−910 m. Among them, the key research areas around the tunnel were encrypted, and 533,327 mesh

elements and 391,299 mesh nodes were finally divided. The deep geo-stress field was measured and inverted on the spot: the maximum principal stress was 34 MPa, perpendicular to the tunnel, and the direction was similar to horizontal; the intermediate principal stress was 25 MPa along the tunnel axis; the minimum principal stress was 19 MPa, and the direction was approximately vertical.

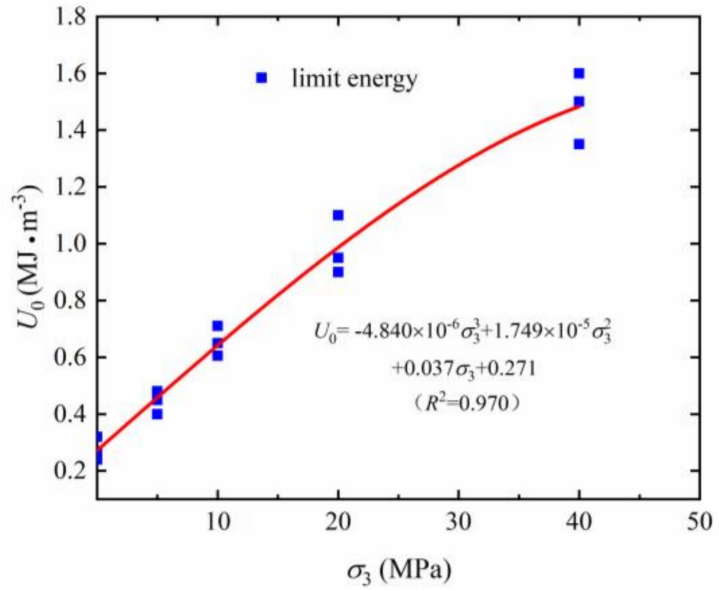

Figure 10. Limiting energy value of granite.

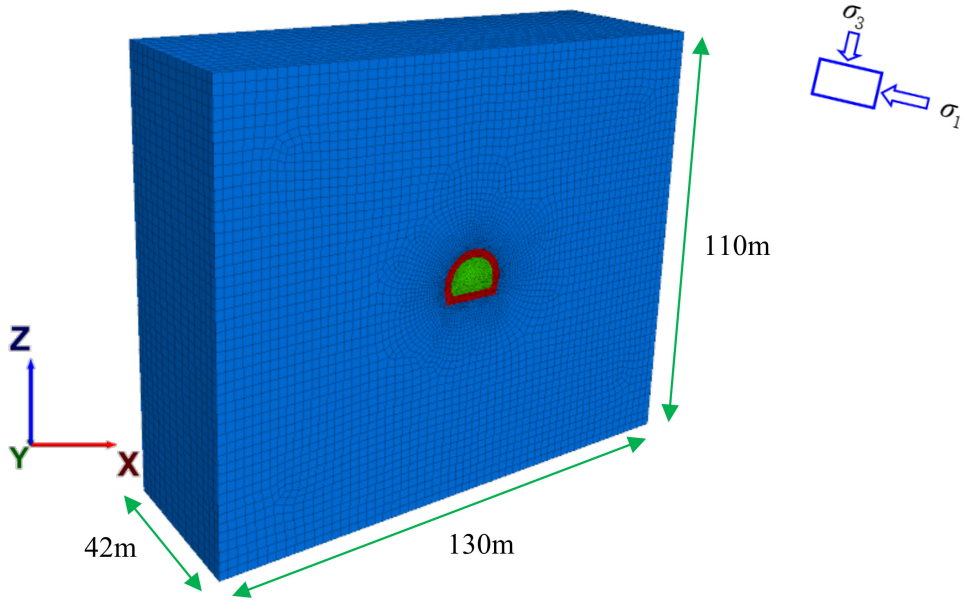

Figure 11. Tunnel calculation model.

Horizontal constraints were used around the model, fixed-end constraints were used at the bottom, and then the gradient ground stress was initialized according to the actual situation. According to the indoor test and the Hoek–Brown criterion, the rock mechanics parameters are shown in Table 7.

Table 7. Calculation parameters of the Wulaofeng tunnel model.

Density g/m^3	Bulk Modulus/GPa	Shear Modulus/GPa	Cohesion/MPa	Friction/°	Principal Stress/MPa
2.71	21.6	14.2	15	48	34-25-19

5.2.2. Analysis of Calculation Results

The tunnel was excavated at 3 m per cycle until the tunnel construction was completed. Energy statistics were performed by writing the fish language to obtain the energy accumulation and change during the excavation process. In order to monitor the energy changes of the elements, monitoring points were arranged at different locations, as shown in Figure 12. The longitudinal spacing of points was 1 m.

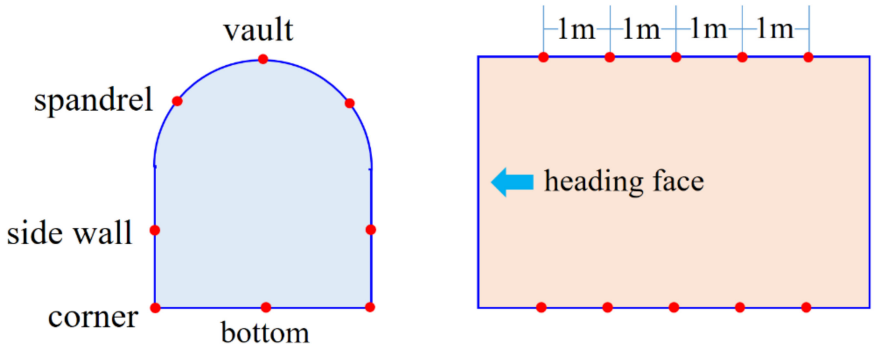

Figure 12. Layout of monitoring points.

The energy distribution of the different stages is shown in Figure 13. When the tunnel was excavated to 36 m, the energy values of measurement points near the free surfacewere extracted to draw curves as shown in Figure 14.

It can be seen from the analysis of Figures 13 and 14 that the initial energy field is relatively uniform, and the stress gravity distribution caused by tunnel excavation leads to changes in the surrounding stress field. After the excavation of the first cycle, there is a significant accumulation of energy around the heading face and at the positions of the spandrel and arch bottom. After the sixth cycle, the energy field has been basically stabilized, and the impact of subsequent construction is minimal, changing slowly. Finally, the energy zone is divided into two parts: the accumulation zone and the low energy zone. There is obvious energy accumulation in tunnel heading face, spandrel and arch bottom, of which the highest accumulation area appears in the left arch bottom with the maximum accumulation energy of 250 kJ. The degree of energy accumulation is greatest at the tunnel surface, and it decreases from the outside to the inside. In the arch bottom, the left side wall, and the spandrel these positions, the strain energy shows a significantly reduced state. With the increase of the distance from the heading face, the accumulated energy of several positions such as the vaults and side walls undergo a process of change from large to small and then increases and stabilizes. In general, there are different degrees of energy accumulation in different locations after the tunnel excavation, which can reflect the destruction trend of the surrounding rock to a certain extent.

Due to the different stress states at each point of the surrounding rock, the limit energy values allowed for storage are also different. Affected by excavation and unloading, the minimum principal stress becomes smaller, and the energy storage limit of the element will be reduced accordingly. When the energy accumulation reaches a certain level and exceeds the energy storage limit, rockburst destruction may occur. From the above energy accumulation analysis, it can be seen that the location of energy accumulation generally occurs near the position of the tunnel surface, and the surrounding pressure of the surface is 0 MPa, so the elements of the air surface position were taken for the limiting energy storage calculation. In order to exclude the abnormal influence of the grid size and the

energy extremes of individual elements, the average energy within the area was taken during calculation.

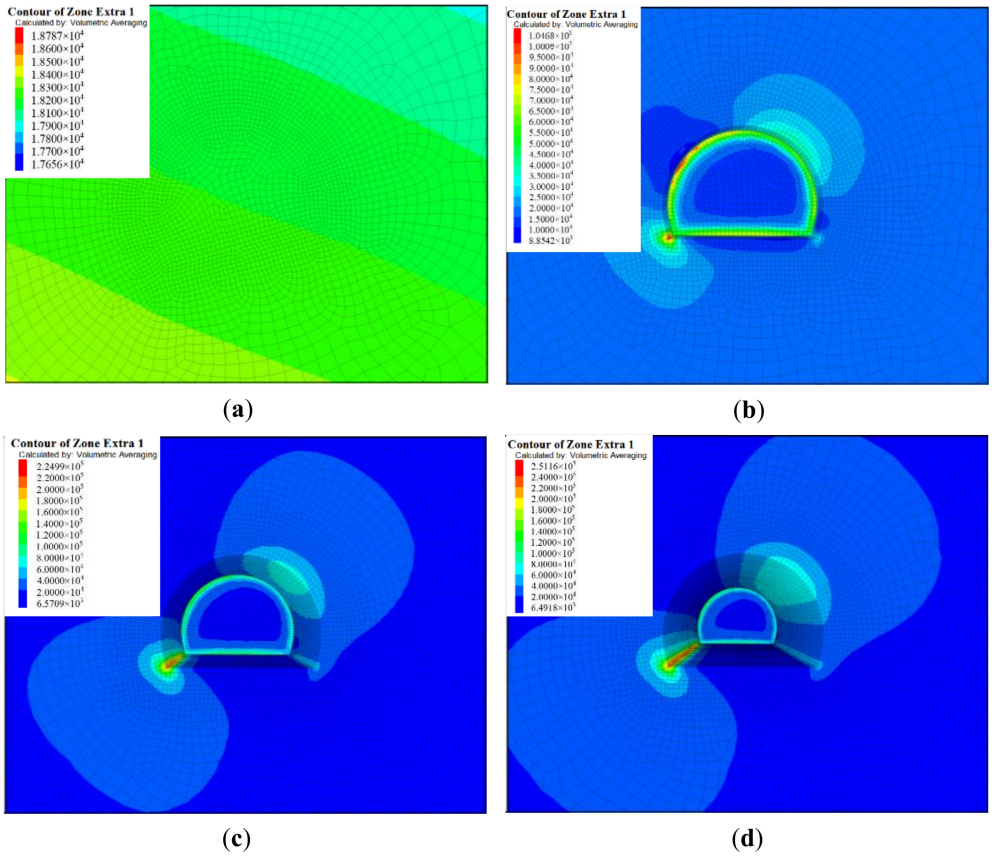

Figure 13. Cloud image of strain energy accumulation in different excavation stages: (**a**) Initial energy field; (**b**) Energy field of cycle 1; (**c**) Energy field of cycle 6; (**d**) Energy field of cycle 12.

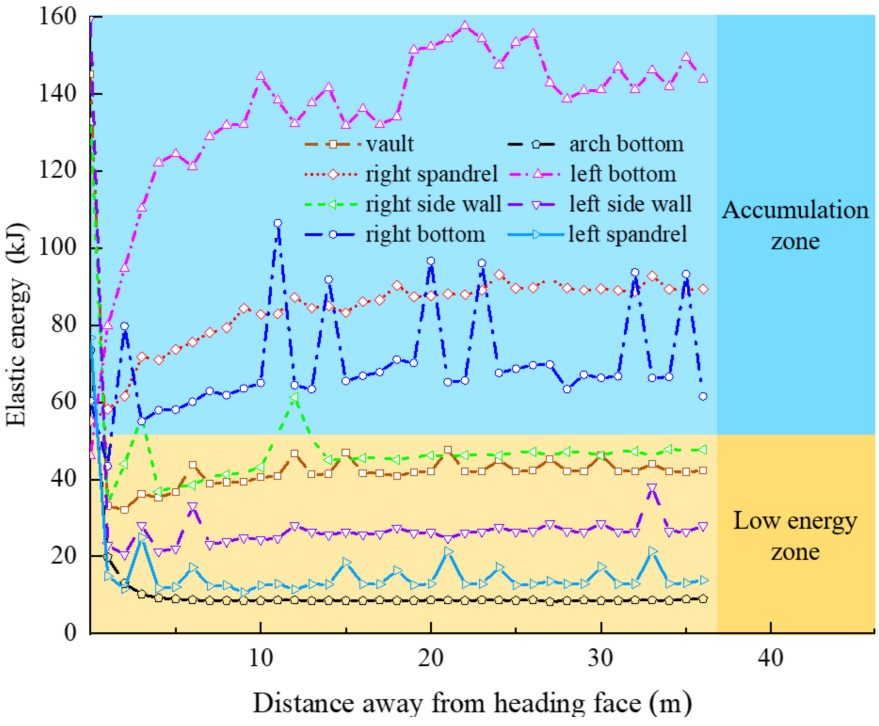

Figure 14. Energy statistics of different measurement points.

Based on a failure criterion of limit energy and numerical simulation, the rockburst tendency of different locations was predicted, and the results are shown in Table 8.

Table 8. Predicted results of rockburst tendency.

Position	U	U/U_0	Judgement Level
Vault	0.11	0.41	medium rockburst
Right spandrel	0.14	0.52	heavy rockburst
Right side wall	0.11	0.43	medium rockburst
Right arch bottom	0.12	0.47	medium rockburst
arch bottom	0.04	0.14	no rockburst
Left arch bottom	0.17	0.65	heavy rockburst
Left Side wall	0.08	0.33	weak rockburst
Left spandrel	0.07	0.25	no rockburst

As seen from Table 8, the deep-buried section of the tunnel has a moderate–heavy risk of rockbursts, especially in the positions of the right spandrel and left arch bottom where strong rockburst will occur, which is basically consistent with the scene situation. No significant rockburst is seen at left and right bottom in site, possibly due to the backpressure of the slag cover. On the whole, attention should be paid to rockburst problems on the site. It is necessary to adopt construction schemes for rockburst prevention and control, such as the timely adoption of drilling and pressure relief, improvement of support measures and safety monitoring to ensure safe construction.

6. Conclusions

In this paper, a wireless hollow envelope stress gauge at great depth was used to measure the geostress in Wulaofeng Tunnel, and mechanical tests and SEM scans were performed on rock specimens obtained from different burial depths. Based on the analysis of SEM, the rockburst mechanism was explored from a microscopic perspective. Based on geo-stress measurements, rock mechanical tests and numerical simulation, the rockburst tendency was comprehensively judged. The main conclusions are as follows:

(1) The geostress field in the deep-buried section of the tunnel is dominated by horizontal stress, and the maximum geostress value reaches 37–40 MPa; rocks from different buried depths both show a certain rockburst tendency from moderate to heavy, and the tendency in depth is slightly greater. However, the rockburst grades are very different: there is no rockburst at the shallow section, while the grade at the deep-buried section varies from weak to strong.

(2) The fractured morphology of granite is mainly of a foliated structure and a block structure, corresponding to the transgranular fractures and intergranular fractures, and the macroscopic manifestation is tension failure. Microscopic components have a certain influence on rockbursts; rocks with few types of mineral cementation, good crystallization degree and small particle size differences have better characteristics of enessrgy storage and release.

(3) The rockburst tendency was judged comprehensively and divided into three stages: analysis of rockburst tendency, prediction of rockburst grade, and analysis of numerical simulation. A variety of criteria were used to comprehensively evaluate the tendency of different buried rocks, avoiding the one-sidedness of a single criterion. The energy zone of the numerical model was divided into the accumulation zone and low energy zone. Relying on numerical simulation and limit energy criterion, the rockburst tendency at different positions of the cross-section was analyzed. The numerical results show the vault, right spandrel and left arch bottom as being more dangerous, which makes the simulation result more targeted.

(4) Through the study of the rockburst mechanism and tendency of the Wulaofeng Tunnel, this provides a basis for rockburst prevention and control measures of the road tunnel, and can provide a certain reference for the analysis of rockburst problems of similar structures.

Author Contributions: J.L. performed the experiments; Y.G. managed research project; F.C. and Z.C. provided research sites and test materials; J.L. wrote original draft. All authors have read and agreed to the published version of the manuscript.

Funding: This research received no external funding.

Data Availability Statement: All representative data are contained in this work.

Acknowledgments: We are grateful to the staff of Wulaofeng Tunnel Project Department for all their technical support and assistance.

Conflicts of Interest: The authors declare no conflict of interest.

References

1. Wang, C.; Cao, C.; Liu, Y.; Li, C.; Lu, H. Experimental investigation on synergetic prediction of rockburst using the dominant-frequency entropy of acoustic emission. *Nat. Hazards* **2021**, *108*, 3253–3270. [CrossRef]
2. Du, H.; Song, D.; Chen, Z.; Guo, Z. Experimental study of the influence of structural planes on the mechanical properties of sandstone specimens under cyclic dynamic disturbance. *Energy Sci. Eng.* **2020**, *8*, 4043–4063. [CrossRef]
3. Zhou, B.; Xu, J.; Peng, S.; Yan, F.; Ni, G. Experimental Analysis of the Dynamic Effects of Coal–Gas Outburst and a Protean Contraction and Expansion Flow Model. *Nat. Resour. Res.* **2010**, *29*, 1617–1637. [CrossRef]
4. Du, H.; Song, D. Investigation of failure prediction of open-pit coal mine landslides containing complex geological structures using the inverse velocity method. *Nat. Hazards* **2022**, *111*, 2819–2854.
5. Aki, K. Generation and propagation of G waves from the Niigata Earthquake of June 16, 1964. Part 2. Estimation of earthquake movement, released energy, and stress-strain drop from the G wave spectrum. *Bull. Earthq. Res. Inst.* **1966**, *44*, 73–88.
6. Wang, H.; Li, Z.; Song, D.; He, X.; Aleksei, S.; Majid, K. An Intelligent Rockburst Prediction Model Based on Scorecard Methodology. *Minerals* **2019**, *9*, 1294. [CrossRef]
7. Feng, X.; Xiao, Y.; Feng, G.; Yao, Z.; Chen, B.; Yang, C.; Su, G. Study on the development process of rockbursts. *Chin. J. Rock Mech. Eng.* **2019**, *38*, 649–673.
8. Zhang, C.; Liu, N.; Chu, W.; Ni, S. Inducement mechanism and case analysis of tectonic rockburst in Jinping II deep buried tunnel. *Chin. J. Rock Mech. Eng.* **2015**, *34*, 2242–2250.
9. Han, X.; Liang, X.; Ye, F.; Wang, X.; Chen, Z. Statistics and construction methods for deep TBM tunnels with high geostress: A case study of Qinling Tunnel in Hanjiang-Weihe River Diversion Project. *Eng. Fail. Anal.* **2022**, *138*, 106301. [CrossRef]
10. Yan, Z.; Liu, D.; Wang, Z.; Zhao, D.; Tian, H. Research on the Method and Model for Calculating Impact Load in the Rockburst Tunnel. *Minerals* **2022**, *12*, 13. [CrossRef]
11. He, M.; Xia, H.; Jia, H.; Jia, X.; Gong, W.; Zhao, F.; Liang, K. Studies on classification, criteria and control of rockbursts. *J. Rock Mech. Geotech. Eng.* **2012**, *4*, 97–114. [CrossRef]
12. Miao, S.; Cai, M.; Guo, Q.; Huang, Z. Rockburst prediction based on in-situ stress and energy accumulation theory. *Int. J. Rock Mech. Min. Sci.* **2016**, *83*, 86–94. [CrossRef]
13. Gu, M.; He, F.; Chen, C. Study on Rockburst in Qingling Tunnel. *Chin. J. Rock Mech. Eng.* **2002**, *21*, 1324–1329.
14. Li, T.; Meng, L.; Wang, L. *High Geostress Tunnel Stability and Rockburst and Large Deformation Disaster Prevention*; Science Press: Beijing, China, 2016.
15. Shan, Z.; Peng, Y. Management of Rock Bursts during Excavation of the Deep Tunnels in Jinping II Hydropower Station. *Bull. Eng. Geol. Environ.* **2010**, *69*, 353–363. [CrossRef]
16. Xu, L. Research on the experimental rock mechanics of rockburst under unloading condition. *J. Chongqing Jiaotong Univ.* **2003**, *22*, 1–4.
17. Zhao, X.; Wang, J.; Cai, M.; Su, G. Influence of Intermediate Principal Stress on the Strainburst Characteristics of Beishan Granite with Consideration of End Effect. *Rock Mech. Rock Eng.* **2021**, *54*, 4771–4791. [CrossRef]
18. Ma, T.; Tang, C.; Tang, S.; Kuang, L.; Yu, Q.; Kong, D.; Xu, Z. Rockburst mechanism and prediction based on microseismic monitoring. *Int. J. Rock Mech. Min. Sci.* **2018**, *110*, 177–188. [CrossRef]
19. Wang, J.; Chen, G.; Xiao, Y.; Li, S.; Chen, Y.; Qiao, Z. Effect of structural planes on rockburst distribution: Case study of a deep tunnel in Southwest China. *Eng. Geol.* **2021**, *292*, 106250. [CrossRef]
20. Luo, Z.; Li, J.; Tang, S.; Li, S.; Zhang, L. Numerical Studies on Rockbursts in Tunnels with High In Situ Stresses and Geothermally Rich Areas. *Appl. Sci.* **2022**, *12*, 5108. [CrossRef]
21. Akdag, S.; Karakus, M.; Taheri, A.; Nguyen, G.; He, M. Effects of Thermal Damage on Strain Burst Mechanism for Brittle Rocks Under True-Triaxial Loading Conditions. *Rock Mech. Rock Eng.* **2018**, *51*, 1657–1682. [CrossRef]
22. Li, T.; Pan, H.; Chen, G.; Meng, L. Physical model tests on thermo-mechanical effects in rockbursts around tunnels. *Chin. J. Rock Mech. Eng.* **2018**, *37*, 261–273.
23. He, M.; Miao, J.; Feng, J. Rock burst process of limestone and its acoustic emission characteristics under true-triaxial unloading conditions. *Int. J. Rock Mech. Min. Sci.* **2010**, *47*, 286–298. [CrossRef]
24. Wang, M.; Zhu, Z.; Liu, J. The photoelastic analysis of stress intensity factor for cracks around a tunnel. *Appl. Mech. Mater.* **2012**, *142*, 197–200. [CrossRef]

25. Li, N.; Feng, X.; Jimenez, R. Predicting rock burst hazard with incomplete data using Bayesian networks. *Tunn. Undergr. Space Technol.* **2017**, *61*, 61–70. [CrossRef]
26. Xue, Y.; Bai, C.; Kong, F.; Qiu, D.; Li, L.; Su, M.; Zhao, Y. A two-step comprehensive evaluation model for rockburst prediction based on multiple empirical criteria. *Eng. Geol.* **2020**, *268*, 105515. [CrossRef]
27. Zhou, J.; Li, X.; Mitri, H.S. Evaluation Method of Rockburst: State-of-the-art Literature Review. *Tunn. Undergr. Space Technol.* **2018**, *81*, 632–659. [CrossRef]
28. Qu, H.; Zhang, X.; Zhang, Y.; Chen, S.; Wu, K. Rock Burst in Deep-buried Tunnel Based on Tendency Index. *Chin. J. Underg. Space Eng.* **2021**, *17*, 949–955.
29. Wu, W.; Xie, X.; Hu, Y.; Chen, J.; Ou, Y. Rock burst proneness in Zhazixi Antimony Mine. *Min. Metall. Eng.* **2017**, *37*, 21–24.
30. Zhang, C.; Yu, J.; Chen, J.; Lu, J.; Zhou, H. Evaluation method for poten-tial rockburst in underground engineering. *Rock Soil Mech.* **2016**, *37*, 341–349. [CrossRef]
31. Guo, B.; Dong, W.; Bo, G.; Si, J. Modifying rock burst criteria based on observations in a di-vision tunnel. *Eng. Geol.* **2017**, *216*, 153–160. [CrossRef]
32. Liu, Z.; Yuan, Q.; Li, J. Application of fuzzy probability model to prediction of rockburst intensity. *Chin. J. Rock Mech. Eng.* **2008**, *27*, 3095–3103.
33. Yu, H.; Liu, H.; Lu, X.; Liu, H. Prediction method of rockburst proneness based on rough set and genetic algorithm. *J. Coal Sci. Eng.* **2009**, *15*, 367–373. [CrossRef]
34. Wang, Y.; Shang, Y.; Sun, H.; Yan, X. Study of prediction of rockburst intensity based on efficacy coefficient method. *Rock Soil Mech.* **2010**, *31*, 529–534.
35. Li, N.; Jimenez, R. A logistic regression classifier for long-term probabilistic prediction of rock burst hazard. *Nat. Hazards* **2018**, *90*, 197–215. [CrossRef]
36. Zhou, J.; Li, X.; Mitri, H.S. Classification of rockburst in underground projects: Comparison of ten supervised learning methods. *J. Comput. Civil Eng.* **2016**, *30*, 04016003. [CrossRef]
37. Zhou, K.; Lin, Y.; Deng, H.; Li, J.; Liu, C. Prediction of rock burst classification using cloud model with entropy weight. *Trans. Nonferrous Met. Soc. China* **2016**, *26*, 1995–2002. [CrossRef]
38. Wang, J.; Apel, D.B.; Pu, Y.; Hall, R.; Wei, C.; Sepehri, M. Numerical modeling for rockbursts: A state-of-the-art review. *J. Rock Mech. Geotech. Eng.* **2021**, *13*, 457–478. [CrossRef]
39. Hatzor, Y.H.; He, B.; Feng, X. Scaling rockburst hazard using the DDA and GSI methods. *Tunn. Undergr. Space Technol.* **2017**, *70*, 343–362. [CrossRef]
40. Chen, G.; He, M.; Fan, F. Rock burst analysis using DDA numerical simulation. *Int. J. Geomech.* **2018**, *18*, 04018001. [CrossRef]
41. Li, X.; Lan, Y.; Zou, J. A study of rock fractures. *J. China U. Min. Technol.* **1983**, *1*, 15–21.
42. Liu, X.; Lee, C.F. Microfailure mechanism analysis and test study for rock failure surface. *Chin. J. Rock Mech. Rock Eng.* **1997**, *16*, 509–513.
43. Cai, M.; Wang, J.; Wang, S. Analysison energy distribution and prediction of rock burst during deep mining excavation in Linglong Gold Mine. *Chin. J. Rock Mech. Rock Eng.* **2001**, *20*, 38–42.
44. Kidybinski, A. Bursting liability indices of coal. *Int. J. Rock Mech. Min. Sci.* **1981**, *18*, 295–304. [CrossRef]
45. Tang, L.; Wang, W. New rock burst proneness index. *Chin. J. Rock Mech. Rock Eng.* **2002**, *21*, 874–878.
46. Wu, S.; Li, L.; Zhang, X. *Rock Mechanics*; Higher Education Press: Beijing, China, 2021.
47. Russenes, B.F. Analyses of Rockburst in Tunnels in Valley Sides (in Norwegian). Ph.D. Thesis, Norwegian Institute of Technology, Trondheim, Norway, 1974.
48. Barton, N.; Lien, R.; Lunde, J. Engineering classification of rock masses for the design of tunnel support. *Rock Mech.* **1974**, *6*, 189–236. [CrossRef]
49. Solecki, R.; Conant, R.J. *Advanced Mechanics of Materials*; Oxford University Press: London, UK, 2003.
50. Chen, W.; Lu, S.; Guo, X.; Qiao, C. Research on unloading confining pressure tests and rockburst criterion based on energy theory. *Chin. J. Rock Mech. Eng.* **2009**, *28*, 1530–1540.
51. Xie, H.; Ju, Y.; LI, L. Criteria for strength and structural failure of rocks based on energy dissipation and energy release principles. *Chin. J. Rock Mech. Eng.* **2005**, *24*, 3003–3010.